EUROFUSION WPPFC-PR(16) 14891

R Mateus et al.

Thermal and chemical stability of the beta-W2N nitride phase

Preprint of Paper to be submitted for publication in
22nd International Conference on Plasma Surface Interactions
in Controlled Fusion Devices (22nd PSI)

This work has been carried out within the framework of the EUROfusion Consortium and has received funding from the Euratom research and training programme 2014-2018 under grant agreement No 633053. The views and opinions expressed herein do not necessarily reflect those of the European Commission.

Thermal and chemical stability of the β-W_2N nitride phase

R. Mateus[a,*], M.C. Sequeira[a], C. Porosnicu[b], C.P. Lungu[b], A. Hakola[c], E. Alves[a]

[a]*Instituto de Plasmas e Fusão Nuclear, Instituto Superior Técnico, Universidade de Lisboa, Av. Rovisco Pais, 1049-001, Lisboa, Portugal*

[b]*National Institute for Lasers, Plasma and Radiation Physics, Bucharest 077125, Romania*

[c]*VTT Technical Research Centre of Finland Ltd, Finland*

*corresponding author: rmateus@ipfn.ist.utl.pt

Abstract

Pure Be, W and Be:W mixed coatings with nominal compositions of (5:5) and (1:9) were deposited on silicon plates and implanted at room temperature with 30 keV N^+ ions with fluences up to 5e17 ions/cm^2. Ion beam and X-ray diffraction analysis evidenced the formation of the α-Be_3N_2 and β-W_2N nitrides. The identified tungsten nitride phase evolves from a BCC W lattice to a BCC W(N) solid solution after irradiating at a fluence of 1e17 N^+/cm^2 and to the compact FCC β-W_2N structure at 5e17 N^+/cm^2. Thermal stability of β-W_2N was investigated by annealing the coatings for 1 hour up to 1073 K. The results point to the release of non-bonded nitrogen solute in β-W_2N over the annealing range and to the thermal stability of the nitride phase up to 1073 K.

Keywords: beryllium, tungsten, nitride, thermal stability

1. Introduction

The first wall of the International Thermonuclear Experimental Reactor (ITER) will use beryllium (Be) and tungsten (W) as plasma facing materials (PFM) in the first wall and divertor, respectively. Be particles eroded from the first wall will be mainly guided by the magnetic field towards the divertor and the composition of this area will evolve significantly over time during the reactor operation, leading to the formation of Be-W mixed layers with different stoichiometries [1]. Another source of co-deposits could be the injection of seeding gases as nitrogen (N) to reduce the power heat loads in the divertor target, while a significant part of the seeding impurities will be accelerated and co-deposited with the Be-W layers [2]. Due to the affinity of N to react with Be and W, the use of N as seeding gas will result in the formation of nitrides [2-4] and it is important to identify the composition and thermal stability of the new phases in order to predict the behaviour of PFM over time under irradiation and annealing. WN_x protective films are

commonly used in other research domains due to their extreme hardness, high electrical conductivity or high chemical stability. The particular formation of tungsten nitrides may result in a decrease of the erosion rates, enhancing the lifetime of the exposed surfaces [5]. Previous experiments revealed that the irradiation of pure Be and W films at low temperature with high fluences of N ions lead to fast saturation of the exposed surfaces such that the thickness of the enriched layers is comparable to the in-depth range of the impinging ions [3,4]. Experiments performed at elevated irradiation energies are important for the research community since abnormal plasma instabilities will easily accelerate particles or runaway electrons towards the divertor region [6]. The implantation of N ions on pure Be with incident energies up to 2.5 keV per atom resulted in the formation of a saturated and thermally stable α-Be_3N_2 superficial layer up to a temperature of 1000 K [3]. For the case of pure W coatings, the irradiation with N ions with energies up to 5 keV per atom evolved to a saturated WN layer, which becomes unstable under annealing at temperatures higher than 600 K [4]. The results agree with the available thermodynamic data. Two beryllium nitride phases with similar standard enthalpies of formation are identified in the binary Be-N diagram: cubic α-Be_3N_2 remains stable from room temperature up to about 1700 to or 1800 K ($\Delta H_{f,298}$ = -589 kJ/mol) and hexagonal β-Be_3N_2 is typically formed at normal pressure and higher temperatures ($\Delta H_{f,298}$ = -572 kJ/mol) [3,7]. Two tungsten nitride phases are also present in the W-N binary system: hexagonal WN, from room temperature up to about 600 K ($\Delta H_{f,298}$ = -24 kJ/mol), and cubic β-W_2N, which typically grows at higher temperatures ($\Delta H_{f,298}$ = -72 kJ/mol) [8]. The thermal stability of the β-W_2N phase remains an open question although it is thought that a new phase transition should only occur at extremely high temperatures [4,8]. Other open question is the possibility to have preferential growth of beryllium nitrides rather than those of tungsten, since they present much lower heats of formation (ΔH_f). A third parameter that may modify the final composition of the nitrides is the energy of the N impinging ions, since higher incident energies lead to deeper ranges of N ions within the targets and possibly, to an increment in the final W/N elemental ratios, retarding the saturation threshold for N [9]. The reaction kinetics involving energetic ions is also favourable to the formation of compounds at temperatures lower than those ones predicted by the available phase diagrams and, moreover, it was already identified the simultaneous growth of both WN and W_2N nitride phases in PFM [10]. The aim of the present experiment was to investigate the growth and thermal stability of nitride phases in mixed Be-W layers by implanting N ions at elevated incident energies. In particular, it should be interesting to observe the formation of tungsten nitrides in the presence of a significant Be content.

2. Experiment and methods

Pure Be, W and mixed Be:W coatings with stoichiometric ratios of (5:5) and (1:9) were deposited by the thermionic vacuum arc method [11,12] on mirror quality silicon (Si) plates with nominal thicknesses of 300 and 400 nm. With the purpose to investigate the reactivity of the Be:W films with nitrogen, in a first campaign the coatings were irradiated with 30 keV N^+ ions at room temperature with nominal fluences of

1e17 and 5e17 ions/cm^2 and current densities of 3.2 μA/cm^2. At this incident energy, the calculated in-depth (Rp) and straggling ranges (ΔRp) of N^+ ions inside the films are about 85 nm and 21 nm for pure Be and of 29 nm and 16 nm for pure W, respectively, assuring that the implantation depth range remains inside the Be:W layers and is not dependent of the substrate composition [9]. From the first irradiation campaign the formation of the β-W_2N phase was identified in all the films containing W, which motivated us for a second set of experiments with the purpose of evaluating the thermal stability of the nitride phase. At this time, Be:W (5:5), Be:W (1:9) and pure W coatings were implanted once again with 30 keV N^+ ions at room temperature with a fluence of 5e17 ions/cm^2 and a current density of 5.0 μA/cm^2, and annealed afterwards in vacuum in the temperature range 573 K to 1073 K with steps of 100 K over 1 h and a base pressure close to 1e-7 mbar. Before and after the implantation campaigns, the thickness of the coatings and the elemental depth profiles of both W and Si were quantified by Rutherford backscattering spectrometry (RBS) using 2.0 or 2.2 MeV $^4He^+$ incident beams. Additionally, the Be, N and O depth profiles were evaluated by Elastic backscattering spectroscopy (EBS) making use of 1.0 to 1.6 MeV H^+ ion beams in order to enhance the backscattering yield of light elements [13,14]. The EBS analysis is particularly useful to evaluate any release mechanism of N induced during the annealing route. Finally, the formation of the nitride phases was identified by X-ray diffraction (XRD) performed in a grazing geometry in order to enhance the pattern yields arising from the thin coatings and mitigate the influence of the substrates. The method is particularly useful for the present investigation, since the unit cells of light compounds as beryllium nitrides induce predominant incoherent scattering, leading to weaker patterns [15]. In this sense, the sensitivity of the XRD analysis is really enhanced in thicker coatings, which is typically obtained by using higher irradiation energies [9,15]. The diffraction patterns were identified by the ICDD data library [16].

3. Results and discussion

3.1 Nitride formation at room temperature

As an example of the analytical procedure, Fig. 1a presents EBS spectra collected from a Be:W (1:9) coating before and after implantation by using a 1.0 MeV H^+ ion beam. The isolated W backscattering yield is identified at higher energies and the inelastic scattering of incident protons by ^{9}Be and ^{14}N becomes visible and superimposed with the backscattering yield of Si from the substrate. The energies corresponding to the presence of N and W in the surface layers are indicated by vertical arrows. The elemental depth quantification of the samples prove that the retention rate of N is higher in the Be coatings: close to 1.00 and 0.95 after irradiation with fluences of 1e17 N^+/cm^2 and 5e17 N^+/cm^2, respectively (the corresponding spectra are not presented in Fig. 1). For the other target compositions the final N content significantly decreases by increasing the W amounts. The RBS spectra obtained from the Be:W (1:9) coatings by using 2.0 MeV ion beams are presented in Fig. 1b. A smooth fluctuation can be seen in the W profile arising from the deposition procedure. Nevertheless, the W depth profile is quite uniform and after N irradiation, it deeply decreases at the surface layers due to the addition of N, and it is possible to evaluate the depth of the

implantation zone using this variation. Apart from the Be coatings, we also notice that the thickness of the remaining targets are not significantly affected by erosion, typically due to the scattering caused by heavy W at the surface. The same mechanism may explain the lower N contents in these samples. Table 1 summarises the quantitative results of the analysis.

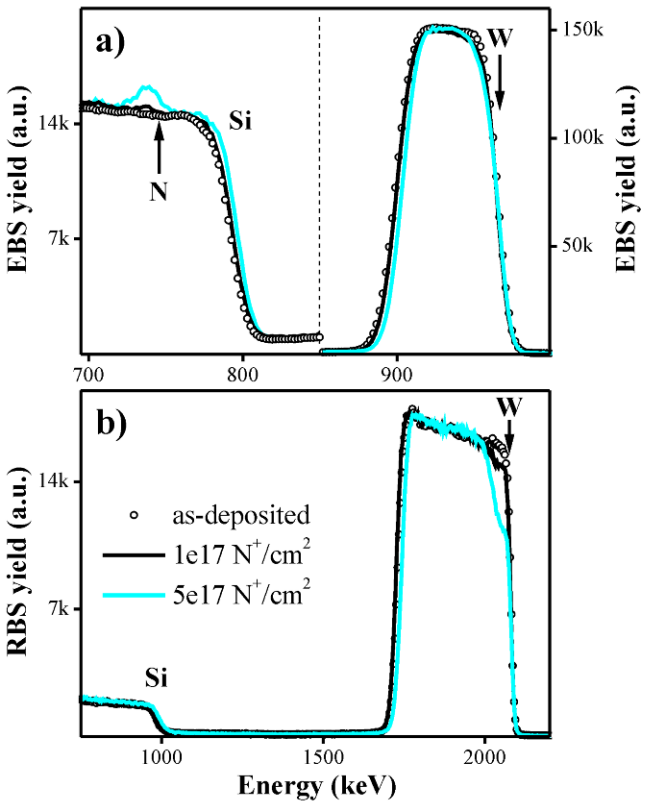

Fig. 1. EBS (a) and RBS (b) spectra collected from Be:W (1:9) before and after N^+ irradiation.

Table 1. Thickness and elemental contents of the implantation zone under N^+ irradiation (estimated error of 5 %).

Be:W sample ($1e17 N^+/cm^2$)		Thickness ($1e17 at/cm^2$)	Be	W	O	N	N ($1e17 at/cm^2$)
			(at.%)				
Be	as-dep.	-	100	-	0	-	-
	1	670	68	-	17	15	1.00
	5	1200	40	-	20	40	4.80
Be:W	as-dep.	-	52	48	0	-	-
(5:5)	1	600	50	38	0	12	0.72
	5	750	38	22	0	40	3.00
Be:W	as-dep.	-	10	90	0	-	-
(1:9)	1	400	8	74	0	18	0.72
	5	510	10	40	0	50	2.55
W	as-dep.	-	-	100	0	-	-
	1	360	-	82	0	18	0.65
	5	450	-	46	0	54	2.43

Fig. 2a presents the diffractograms obtained from Be coatings, before and after 30 keV N^+ implantation with nominal fluences of 1e17 and 5e17 N^+/cm^2. The sensitivity to detect light elements and compounds in thin films by XRD is very low [15]. Nevertheless, the characteristic peak lines for Be become visible at 45.8°,

50.9°, 52.8° and also at 70.8°, corresponding to the diffraction pattern for the planes (100), (002), (101) and (102). After irradiation at 5e17 N^+/cm^2, a new and broad yield becomes visible close to 38.2°, as it was confirmed from an additional XRD scan performed at the same angular range, and the result is compatible with the diffraction peak for cubic α-Be_3N_2 at the (222) plane [3]. The presence of heavy W makes it impossible to distinguish Be or Be_3N_2 patterns in the diffractograms of Fig. 2b and 2c [15]. For the as-deposited Be:W (5:5) coating (Fig. 2b) we identify the characteristic W pattern at 40.3° for the (110) plane, where the scattering yield for W is typically more intense, and also at 58.3° (200) and 73.2° (211). After the exposure of 5e17 N^+/cm^2 the β-W_2N pattern is easily identified at 37.8° (111), 43.9° (200) and 63.9° (220). The W and β-W_2N phases are also identified in the diffractograms related to Be:W (1:9) (Fig. 2c), and in pure W (Fig. 2d), and obviously, the W peaks are more intense in this coatings, due to the increment of the W content. Therefore, we are more sensitive to observe the changes involving the W component in these batches.

After irradiating the W and Be:W (1:9) coatings with a fluence of just 1e17 N^+/cm^2, a new diffraction peak appears at an angle 2θ close to 38.8° overlapping with the peak line of the (110) plane for W at 40.3° (Fig. 2c and 2d). Apart from the Si component, which remains in the substrate and is not visible in the diffractograms by grazing XRD, the change could be only explained by the addition of N atoms in the unit cell of W. From the Bragg's law, and considering the wavelength of 0.154 nm for the Cu $K_{\alpha 1}$ line of the X-ray source, an angular deviation from 40.3° to 38.8° corresponds to the increment of the lattice parameter *a* for W from 0.317 nm, the reference for pure BCC W [16], to about 0.328 nm, corresponding to a swelling behaviour close to $\Delta a/a \cong 3.5$ %. The result agrees with the formation of a BCC W(N) solid solution inside the implantation zone, in the region of 50-100 nm, as predicted by the calculations using the SRIM code [9]. Therefore, patterns relative to pure W from deeper layers inside the coatings are also present in the diffractograms. Afterwards, at a fluence of 5e17 N^+/cm^2 the new peak vanishes and gives rise to the cubic β-W_2N pattern, which has a more compact FCC structure. The intensities of the β-W_2N peaks in the diffractograms of Fig. 2c and 2d are lower than those ones observed in Fig. 2b for the Be:W (5:5) stoichiometry, and the difference may be justified by the low N content of the samples (see Table 1) or by a lower medium size of the β-W_2N grains [15].

The formation of solid solutions by N addition could be also identified from Fig. 2a, where the reported value for 2θ relative to plane (222) in the α-Be_3N_2 lattice is about 38.2° [16]. Nevertheless, the corresponding value observed from Fig. 2a is lower and close to 37.8°, and agrees with the increment of the lattice constant *a* of α-Be_3N_2 by factor of $\Delta a/a \cong 1$ % after the implantation of 5e17 N^+/cm^2, and to the presence of an α-Be_3N_2 (N) solution.

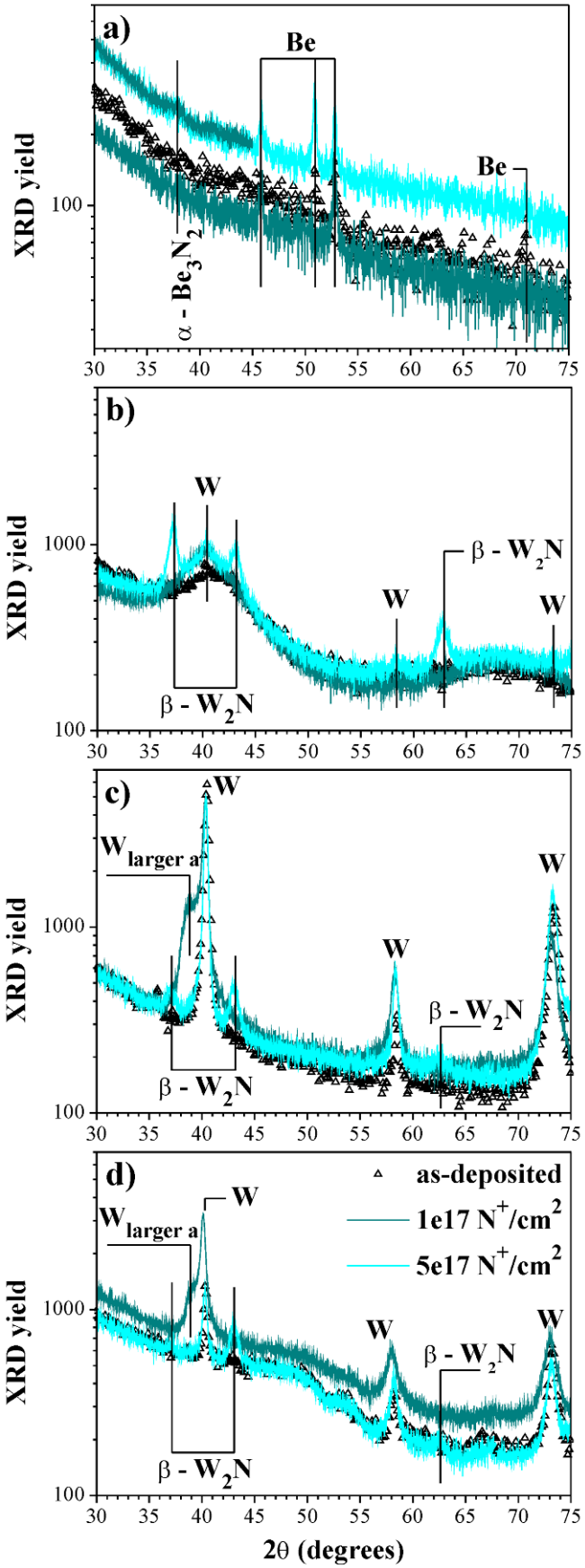

Fig. 2. X-ray spectra of Be:W batches before and after N^+ implantation on Be (a), Be;W (5:5) (b), Be;W (1:9) (c) and W (d).

3.2 Thermal stability of β-W_2N

EBS and RBS spectra of the films were collected before and after implantation and during the annealing procedure from the incidence of 1.6 MeV H^+ and 2.2 MeV He^+ ion beams, respectively. Changes in the elemental depth profiles were not significant by annealing up to 873 K the Be:W (1:9) and the W samples and therefore Fig. 3 summarises the evolution of spectra from a W sample after implantation and after annealing at 873 and 1073 K. The retention of N in the implantation zone is identified in the EBS spectra of Fig. 3a by the vertical arrow nearby 1200 keV. The N yield is significant after implantation and smoothly decreases from 873 to 1073 K. The same behaviour can be seen for the Be:W (1:9) samples. In contrast, a fast decrease and spread of the N yield is observed by annealing the Be:W (5:5) samples up to 873 K. Possibly, the behaviour is induced by an increment in the surface roughness under thermal stress due to the simultaneous and competitive growth of hexagonal BeO, with a heat of formation ($\Delta H_{f,298}$ = -608 kJ/mol) similar to that one of cubic α-Be_3N_2 ($\Delta H_{f,298}$ = -572 kJ/mol), and of cubic β-W_2N. The same behaviour explains the final delamination of the films at 973 K [17]. Fig. 3b presents RBS spectra collected from the W coatings before and after annealing at the same temperatures. The depth profiles of W are quite similar for the as deposited samples and for the samples annealed at 873 K, and at 973 and 1073 K a smooth increment in the interdiffusion between Si and W is observed at the interface between the coating and the substrate, proving that the Si component in the substrate did not affect the final results. Simultaneously, the deep decrease in the W profile at the surface layers caused by ion implantation becomes modified at higher temperatures. The change may be explained by an increment in the surface roughness or by the spreading of the impurity location at the surface induced by the growth of oxides or by smooth diffusion of N into the films.

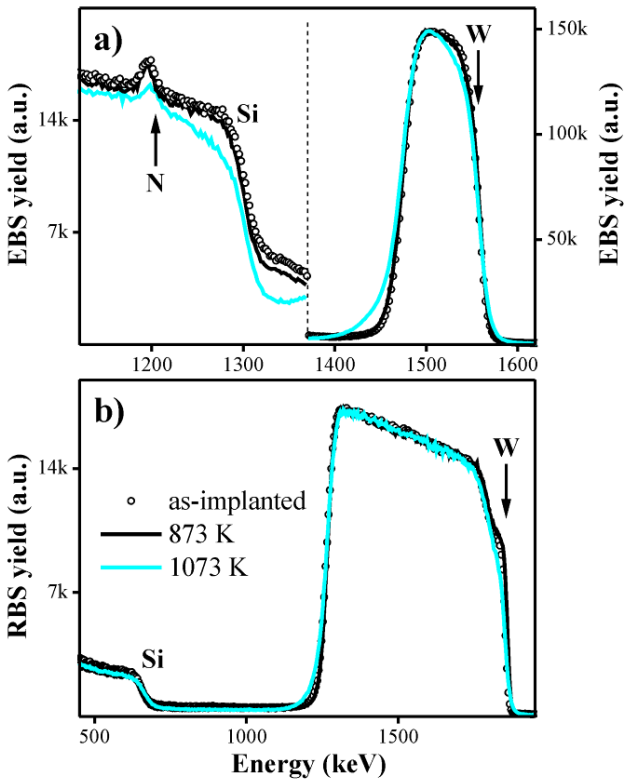

Fig. 3. EBS and RBS spectra collected from pure W coatings during the annealing process.

Table 2 summarises the results of the present analysis. The remaining elemental content relates to oxygen. By comparing the new data with those in Table 1, a decrease in the Be and N contents is observed in the implantation zone after irradiation with a fluence of 5e17 N^+/cm^2, which is explained by the use of a higher current density in the new implantation campaign (5.0 $\mu A/cm^2$ vs. 3.2 $\mu A/cm^2$), enhancing the erosion of the irradiated surfaces. Nevertheless, the smooth decrease in the N amounts did not change the final results, since they are high enough to induce the formation of supersaturated β-W_2N. Taking into account the elemental content quantified by the ion beam data, the available N retained in the W coatings exceeds the required amount imposed by the β-W_2N stoichiometry.

Table 2. Thickness and elemental contents of the implantation zone under N^+ irradiation and annealing (estimated error of 5 %).

Be:W	sample	Thickness	Be	W	O	N	N
5e17N^+/cm^2		(1e17at/cm^2)	(at.%)				(1e17at/cm^2)
Be:W	as-dep.	-	46	54	0	-	-
(5:5)	as-imp.	480	12	40	0	48	2.30
	673 K	480	12	40	4	44	2.11
	773 K	480	12	40	10	38	1.83
Be:W	as-dep.	-	10	90	0	-	-
(1:9)	as-imp.	500	8	44	0	48	2.40
	773 K	500	8	44	0	48	2.40
	873 K	500	8	44	0	48	2.40
	973 K	500	8	44	4	44	2.20
	1073 K	500	8	44	13	35	1.75
W	as-dep.	-	-	100	0	-	-
	as-imp.	460	-	50	0	50	2.30
	773 K	460	-	50	0	50	2.30
	873 K	460	-	50	0	50	2.30
	973 K	460	-	50	6	44	2.02
	1073 K	460	-	50	12	38	1.75

Once again, the diffractograms collected from the as-implanted and annealed Be:W (5:5), Be:W (1:9) and W coatings clearly show that after implantation with a fluence of 5e17 N^+/cm^2 the W pattern evolves along the implantation depth zone from a pure W structure to the β-W_2N phase, and additionally, pure W remains visible in the diffractograms because W does not react with N at deeper depths. Similar conclusions are obtained from all the diffractograms collected along the entire annealing sequence. The area of the diffraction peaks for the β-W_2N phase slightly decreases by increasing the temperature in Be:W (5:5) and possibly, the result is just related to the simultaneous growth of BeO at the surface due to the affinity of Be to react with O [3,17]. Nevertheless, it does not evolve with temperature in Be:W (1:9) and W. The results agree with the ion beam data, pointing to the fact that N does not diffuse deep inside the films, where the excess of N at the surface layers could easily react with pure W. The ion beam results in Table 2 agree with the presence of supersaturated β-W_2N. They also show that the retained N amounts decrease by increasing the annealing temperature. From the XRD spectra, we conclude that the previous results are compatible with the release of non-bound N from the nitride phase, since it is observed a systematic increment of the

diffraction angles 2θ for the β-W_2N pattern along the entire annealing route. As an example, in the (pure) W batch the measured angle 2θ for the diffraction line of the (200) plane evolves from 43.04° in the as-implanted sample to about 43.66° after annealing at 1073 K and the reported angle for the pure β-W_2N phase is 43.80° [16,18]. Therefore, the corresponding increment of the lattice parameter for β-W_2N calculated from the Bragg's law decreases from 1.7 % to about 0.3 % in these samples. Clearly, the results are compatible with the occurrence of a gradual release of unbound N atoms inside the β-W_2N (N) lattice to other locations during the annealing process [19], and at 1073 K some of the excess N content should remain inside the β-W_2N unit cells, since the reported diffraction angle 2θ for the stoichiometric β-W_2N composition is not achieved. Concluding, the results point to the formation of a supersaturated β-W_2N (N) solid solution after implantation of 30 keV N^+ ions with a fluence of 5e17 ions/cm^2 and to the release of non-bound N atoms in the β-W_2N lattice upon annealing. The results also suggest thermal stability of the β-W_2N phase up to 1073 K. The same conclusions are obtained from the analysis of the Be:W (5:5) and Be:W (1:9) coatings.

With the purpose to simplify the information obtained from the new XRD spectra, Fig. 4 presents the variation of the lattice parameter *a* for the β-W_2N phase evaluated for all the Be:W (5:5), Be:W (1:9) and W diffractograms by using the Bragg's law. All the calculations assumed the deviation of the peak line for the (200) plane in β-W_2N. The annealing procedure leads to a regular decrease of the lattice parameter towards the reported reference value, which is not reached after annealing at 1073 K since part of the non-bound N atoms remain inside the β-W_2N unit cell. The same results show that the lattice parameter of the β-W_2N phase slightly decreases in the as-implanted samples by increasing the Be content of the coatings. Possibly, the result is related to a lower amount of non-bonded N atoms inside the β-W_2N unit cell due to the competitive formation of beryllium nitride, which cannot be identified in the diffractograms due to the superposition of both β-W_2N and α-Be_3N_2 pattern yields. The quest should be addressed to further investigations. Nevertheless, it is clearly proved that despite the lower heat of formation of beryllium nitrides, the final β-W_2N content becomes significant by irradiating mixed Be-W layers with energetic N ions. Fig. 4 also presents the corresponding N contents evaluated by EBS. In opposition to the evolution of the lattice parameter *a*, the N amount remains constant in the Be:W (1:9) and W coatings up to 873 K and only decreases at higher temperatures. The results agree with the migration of non-bonded N from the β-W_2N lattice to other locations inside the implantation zone up to 873 K, e.g., in lattice defects along grain boundaries, and to the release of N at high temperatures.

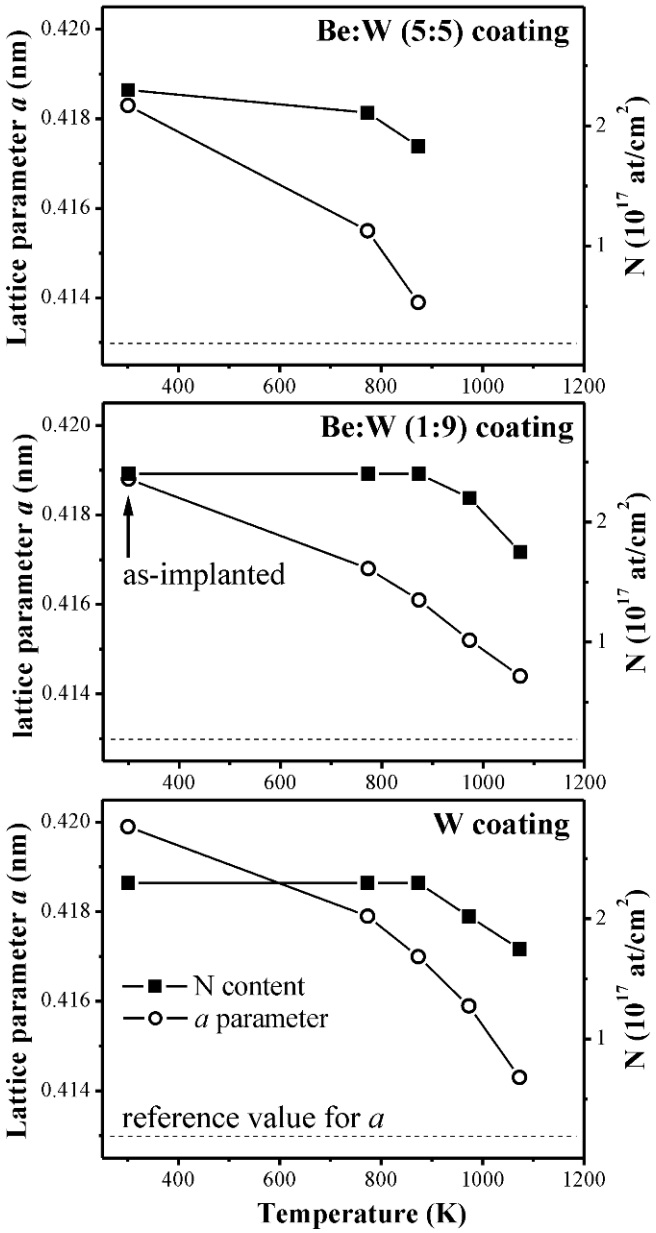

Fig. 4. Lattice parameter *a* of β-W_2N and N contents evaluated from W coatings after N^+ implantation and annealing, as function of the annealing temperature.

4. Conclusions

Pure Be and W and mixed Be-W coatings of different compositions were exposed to energetic N^+ ions, and the formation of both beryllium and tungsten nitride phases was identified in various Be and W samples. Despite a much lower heat of formation of beryllium nitrides, our results show that the irradiation of mixed Be-W layers with N^+ ions (up to 30 keV) leads to the formation of a solid solution of BCC W(N) at lower fluences and to the final compact form of supersaturated β-W_2N (N) at room temperature. The annealing procedure leads to the release of the unbound N content in β-W_2N, and at 1073 K a part of the excess N seems to remain inside the tungsten nitride lattice, which is still present in the coatings. The present results point to the thermal stability of the β-W_2N phase up to 1073 K. Further investigations should be carried out to investigate the competitive formation of both tungsten and beryllium nitride phases in Be-W samples.

Acknowledgements

This work has been carried out within the framework of the EUROfusion Consortium and has received funding from the Euratom research and training programme 2014-2018 under grant agreement No 633053. The activity was performed in the scope of the WP PFC programme. IST also received financial support from "Fundação para a Ciência e a Tecnologia" through project UID/FIS/50010/2013. The views and opinions expressed herein do not necessarily reflect those of the European Commission.

References

[1] R.P. Doerner, The implications of mixed-material plasma-facing surfaces in ITER, J. Nucl. Mater. 363-365 (2007) 32.

[2] M. Oberkofler et al., First nitrogen-seeding experiments in JET with the ITER-like Wall, J. Nucl. Mater. 438 (2013) S258.

[3] M. Oberkofler, Ch. Linsmeier, Properties of nitrogen-implanted beryllium and its interaction with energetic deuterium, Nucl. Fusion 50 (2010) 125001.

[4] K. Schmid et al., Interaction of nitrogen plasmas with tungsten, Nucl. Fusion 50 (2010) 025006.

[5] D. Alegre et al., Characterization of tungsten nitride layers and their erosion under plasma exposure in nano-PSI, Romanian Reports in Physics 67 (2) (2015) 532.

[6] A. Hassanein, I. Konkashbaev, Comprehensive modeling of ELMs and their effect on plasma-facing surfaces during normal tokamak operation, J. Nucl. Mater. 313-316 (2003) 664.

[7] R.C. Ropp, Encyclopedia of the Alkaline Earth Compounds, Elsevier, Amsterdam, 2013.

[8] R. Kieffer, F. Benesovsky, Hartstoffe, Springer-Verlag, Wien, Austria, 1963.

[9] SRIM 2013 software package, http://www.srim.org

[10] M. Rubel, V. Philipps, L. Marot, P. Petersson, A. Pospieszczyk, B. Schweer, Nitrogen and neon retention in plasma-facing materials, J. Nucl. Mater. 415 (2011) S223.

[11] C.P. Lungu et al., Beryllium Coatings on Metals: Development of Process and Characterizations of Layers, Phys. Scr. T128 (2007) 157.

[12] C.P. Lungu et al., The behavior of W, Be and C layers in interaction with plasma produced by terawatt laser beam pulses, Vacuum 110 (2014) 207.

[13] IBANDL data library, http://www-nds.iaea.org/ibandl/

[14] N.P. Barradas, C. Jeynes, R.P. Webb, Simulated annealing analysis of Rutherford backscattering data, Appl. Phys. Lett. 71 (1997) 291.

[15] B.D. Cullity, Elements of X-ray Diffraction, second ed., Addison-Wesley, Reading, Massachusetts, USA, 1978.

[16] ICDD PDF-2 Data library, http://www.icdd.com

[17] R. Mateus et al, Formation and delamination of beryllium carbide films. J. Nucl. Mater. 363-442 (2013) S320.

[18] V.I. Khitrova, Z.G. Pinsker, An electron-diffraction study of cubic tungsten nitride, (1959) (4) 513, Sov. Phys. Crystallogr. (1954) 4, 513.

[19] Y.G. Shen, Y.W. Mai, Microstructure and structure characteristics of cubic WN*x* compounds, Mater. Sci. Eng. A 288 (2000) 47.